Sodium Doped Strontium Silicates as Electrolyte for Intermediate Temperature Solid Oxide Fuel Cells

ECS Transactions, 78 (1) 467-475 (2017)
10.1149/07801.0467ecst ©The Electrochemical Society

Sodium Doped Strontium Silicates as Electrolyte for Intermediate Temperature Solid Oxide Fuel Cells

A. C. Kundur[a], M. P. Singh[b], V. A. Sethuraman[a,b]

[a]Department of Materials Engineering, Indian Institute of Science, Bangalore 560 012, India
[b]Interdisciplinary Centre for Energy Research, Indian Institute of Science Bangalore 560 012, India

The conventional solid oxide fuel cell electrolyte, yttria stabilized zirconia requires high operating temperature (800-1000^{0}C) to achieve sufficient oxide ion conductivity, which increases the cost and exacerbates the instability between the components. Therefore, there is considerable interest in developing alternative electrolytes ($\sigma > 10^{-2}$ S/ cm) at intermediate temperature (IT, 500-700^{0}C). Hence, here we successfully synthesized IT operable electrolytes $Sr_{1-x}Na_xSiO_{3-\delta}$ (x = 0.0, 0.45) by solid state reactions. From the XRD, it is evident that both samples can be indexed to monoclinic *c*2/*c* space group (15). NMR reveals a broad peak at ~ −87 ppm for $Sr_{0.55}Na_{0.45}SiO_{3-\delta}$ indicating the presence of amorphous $Na_2Si_2O_5$ phase. FE-SEM and WDS mapping shows the segregation of amorphous $Na_2Si_2O_5$ along the grain boundaries. $Sr_{0.55}Na_{0.45}SiO_{3-\delta}$ exhibits high conductivity in the measured temperature range, which makes it an electrolyte for IT-SOFCs.

Introduction

Solid oxide fuel cells (SOFCs) are electrochemical devices, which convert the chemical energy to electricity with high efficiency, low pollutant emission and excellent fuel flexibility (1). The most commonly used electrolyte in SOFCs is yttria-stabilized zirconia due to its high oxygen ionic conductivity and compatibility with electrodes at high temperature (HT, 800^{0}C-1000^{0}C) (2). However, such HT leads to thermal degradation, thermal expansion mismatch between the cell components (electrodes-electrolyte), interfacial reaction between the electrodes and electrolyte and high cost of said materials (3). Therefore, decreasing the SOFCs operation temperature from HT to intermediate temperature (IT, 500^{0}C-700^{0}C) is the current trend in SOFC research. By decreasing the operating temperature to IT both ohmic (electrolyte) and polarization (electrode) losses increase significantly. Ohmic loss is reduced by developing new electrolyte materials with high oxygen ionic conductivity at IT and decreasing the electrolyte thickness. The electrode loss can be minimized by optimizing the electrode microstructure and increasing the electrodes activity (4,5). The electrolytes for IT-SOFCs include rare earth doped ceria and magnesium doped lanthanum gallate (LSGM). In rare earth doped ceria, Ce^{4+} can be easily reduced to Ce^{3+} at reducing atmosphere, which induces n-type electronic conduction and causes internal short circuit (6). Problems with LSGM at IT are high cost of gallium, reduction and volatilization of gallium oxides, under oxidizing

conditions a significant reactivity with perovskite electrodes as well as metal anode in reducing conditions (7).

In-order to overcome from the problems associated with existing IT electrolytes, Goodenough et al. introduced layered monoclinic $Sr_{1-X}A_XMO_{3-\delta}$ (A = Na or K, M = Si/Ge) solid solutions as electrolytes for IT-SOFCs (8), and also reported the highest oxygen ionic conductivity for Na doped $SrSiO_3$ among all known stable oxygen ion conductors. In $Sr_{1-X}Na_XSiO_3$, Na doping into $SrSiO_3$ creates oxygen vacancies through which the oxygen ion moves is the main reason for conductivity, which was supported by Xu et al. (9) in $Sr_{1-X}K_XSiO_3$ system. Bayliss et al. (10,11) performed detailed investigations and claims that it would be difficult to dope Na or K into Sr sites in $SrSiO_3$. $Sr_{1-X}Na_XSiO_3$ are mixtures, containing crystalline and amorphous phases. Hence, to identify the exact path of the oxide ion conductivity, whether through the grain or grain boundary in $Sr_{1-X}Na_XSiO_3$ system, in the present work we have synthesized the $Sr_{1-X}Na_XSiO_3$ (x = 0.0 and 0.45) by solid state reaction. Characterized by XRD, ^{29}Si NMR, FE-SEM, WDS, TEM and electrochemical impedance spectroscopy. Here, we also correlate the structural, micro-structural properties of $Sr_{1-X}Na_XSiO_3$ with electrochemical impedance spectroscopy studies. Solid state ^{29}Si NMR for $Sr_{0.55}Na_{0.45}SiO_{3-\delta}$ shows a broad peak at ~ −87 ppm, which indicates the presence of amorphous $Na_2Si_2O_5$. FE-SEM image and WDS mapping clearly shows the presence of two phases in $Sr_{0.55}Na_{0.45}SiO_{3-\delta}$ i.e., Na-$SrSiO_3$ in the grain and $Na_2Si_2O_5$ segregation along the grain boundaries, which is the main reason for conductivity.

Experimental

$SrSiO_3$ and $Sr_{0.55}Na_{0.45}SiO_{3-\delta}$ were synthesized by solid state reaction method. Initially, the starting materials $SrCO_3$, Na_2CO_3, SiO_2 (Sigma Aldrich, purity ≥ 99.99%) were weighed in stoichiometric amount and ground in an agate mortar pestle for 2hr with ethanol as mixing medium. As synthesized powders of $SrSiO_3$ and $Sr_{0.55}Na_{0.45}SiO_{3-\delta}$ were calcined at 1250^0C and 1050^0C for 20 hr respectively in high purity alumina crucibles covered with lids to get final products. Amorphous $Na_2Si_2O_5$ was also synthesized by using stoichiometric amount of Na_2CO_3, SiO_2 and calcined at 950^0C/ 10h. Room temperature powder X-ray diffraction (XRD) of the synthesized samples were carried out in the PAN Analytic X-ray diffractometer using CuKα radiation with the wavelength of 1.5406 Ä. Solid state NMR spectra were acquired on a JEOL, JNM-ECX400II instrument with field strength 9.4 T using HXMAS 4 mm probe. A single pulse and acquisition of ^{29}Si signal was collected using scan number of 4096 at MAS speed 10 kHz at ambient temperature. The spectra were reference with TMS (Tetramethylsilane). The micro-structural features of the sintered pellet/ powder was determined by field-emission scanning electron microscope (FE-SEMCarl Zeiss, Ultra 55) and transmission electron microscope (FEI Tecnai G2 T20 U−Twin TEM). WDS elemental mapping was performed in an electron probe micro-analyzer (EPMA: JEOL JXA8230) equipped with Field Emission Gun (FEG). Samples were coated with thin layer of gold before imaging in EPMA. The conductivity measurements were carried out in air using Autolab (Model 302N) potentiostat in the frequency range 1 MHz to 0.1 Hz. For impedance measurements, the calcined powders were pressed into pellets (10 mm diameter, 2 mm thickness) with 1wt.% poly (vinylbutyral (PVB)) and then firing at 900^0C/ 20 hr. Both sides of the sintered pellets were coated with high temperature silver

paste for electrical contact. Prior to impedance measurement, the temperature was equilibrated for 30 min at each set point and readings were recorded on cooling from $700^0C - 300^0C$.

Results and Discussion

Phase Analysis

Figure 1 shows the room temperature XRD patterns for $SrSiO_3$ and $Sr_{0.55}Na_{0.45}SiO_{3-\delta}$. Here, both the materials are single phase with monoclinic structure (PDF. No.: 36-0018, c2/c space group (15)) (12). The parent $SrSiO_3$ requires high temperature (1250 ^0C) for the removal of impurities like Sr_2SiO_4 and SiO_2 and to achieve the single phase. The broad flat top at $2\theta \sim 15^0$ for $SrSiO_3$ indicate the presence of voids. However, these flat top becomes peaks for $Sr_{0.55}Na_{0.45}SiO_{3-\delta}$. The peak splitting is observed for $Sr_{0.55}Na_{0.45}SiO_{3-\delta}$ corresponding to higher $2\theta > 45^0$, which is due to disorder exerted on parent $SrSiO_3$ (13). The causes for disorder are Na doping into $SrSiO_3$, stress and vacancy formation. In $Sr_{0.55}Na_{0.45}SiO_{3-\delta}$, the growth of the monoclinic phase is controlled by both SiO_2 layers and amorphous SiO_2 matrix, when compare to $SrSiO_3$ where in the monoclinic phase growth is controlled by only SiO_2 layers.

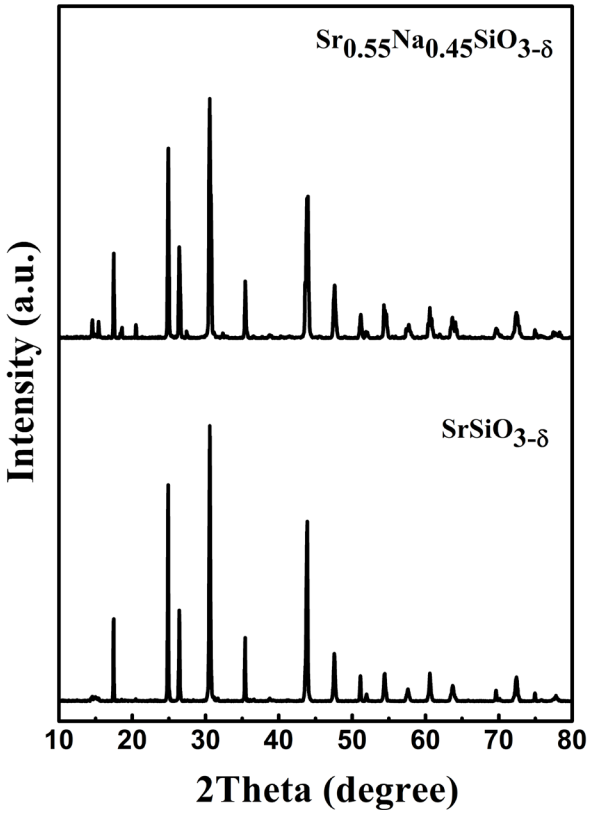

Figure 1. Room temperature XRD patterns for $SrSiO_3$ and $Sr_{0.55}Na_{0.45}SiO_{3-\delta}$.

Solid State ^{29}Si NMR Study

Solid state NMR spectroscopy is a powerful technique which can explains the ion dynamics as well as local defect structure in ion conductors. Figure 2 shows the ^{29}Si

NMR spectra for $SrSiO_3$, $Sr_{0.55}Na_{0.45}SiO_{3-\delta}$ and amorphous $Na_2Si_2O_5$. ^{29}Si NMR spectrum of $SrSiO_3$ exhibits a sharp single peak centered at – 83 ppm, which is due to Si_3O_9 sites in $SrSiO_3$. For $Sr_{0.55}Na_{0.45}SiO_{3-\delta}$, the peak at – 83 ppm is replaced by a broad peak centered at ~ – 87 ppm, which indicate the formation of disordered phase (14). The new disordered phase identified here is amorphous $Na_2Si_2O_5$. In-order to verify the amorphous phase present in $Sr_{0.55}Na_{0.45}SiO_{3-\delta}$, amorphous $Na_2Si_2O_5$ was prepared from solid state reactions. The ^{29}Si NMR spectrum of amorphous $Na_2Si_2O_5$ clearly resembles the broad peak of $Sr_{0.55}Na_{0.45}SiO_{3-\delta}$, which confirms its amorphous nature. These investigations clarifies that Na is hardly substituted into $SrSiO_3$. The amorphous $Na_2Si_2O_5$ is the main reason for enhanced ionic conductivity in $Sr_{0.55}Na_{0.45}SiO_{3-\delta}$.

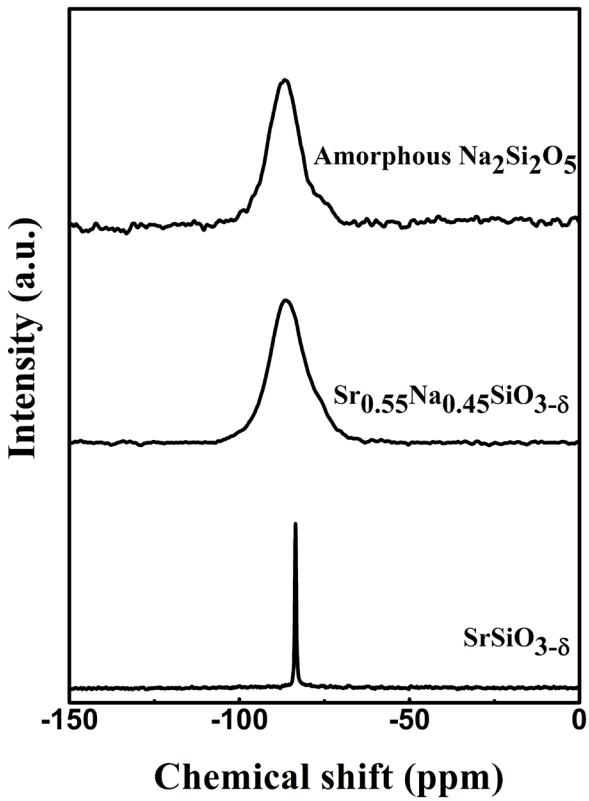

Figure 2. ^{29}Si NMR spectra of $SrSiO_3$, $Sr_{0.55}Na_{0.45}SiO_{3-\delta}$ and amorphous $Na_2Si_2O_5$.

Microstructural Analysis

Figure 3(a) shows the FE-SEM image of the $Sr_{0.55}Na_{0.45}SiO_{3-\delta}$ sintered pellet. Clearly, it contains two phases: liquid phase along the grain boundaries (GBs) and solid phase in the grain. Furthermore, WDS mapping (Figure 3(b-f)) shows the compositional distribution of the sintered pellets, which confirms that the solid phase is sodium deficient (grain) and liquid phase is sodium rich. The sodium segregation along the GBs indicates that, substitution of Na^+ (at high concentration) for Sr^{2+} in $Sr_{0.55}Na_{0.45}SiO_{3-\delta}$ is unfavorable and also the presence of $Na_2Si_2O_5$ at GBs. Hence, $Sr_{0.55}Na_{0.45}SiO_{3-\delta}$ is a mixture of crystalline $SrSiO_3$ and amorphous $Na_2Si_2O_5$. Figure 4 show the TEM image for $Sr_{0.55}Na_{0.45}SiO_{3-\delta}$. It contains the monoclinic structure fringes (marked by white ovals) surrounded by amorphous phase. These observations indicate that, in $Sr_{0.55}Na_{0.45}SiO_{3-\delta}$ amorphous $Na_2Si_2O_5$ is dispersed in a crystalline $SrSiO_3$ phase.

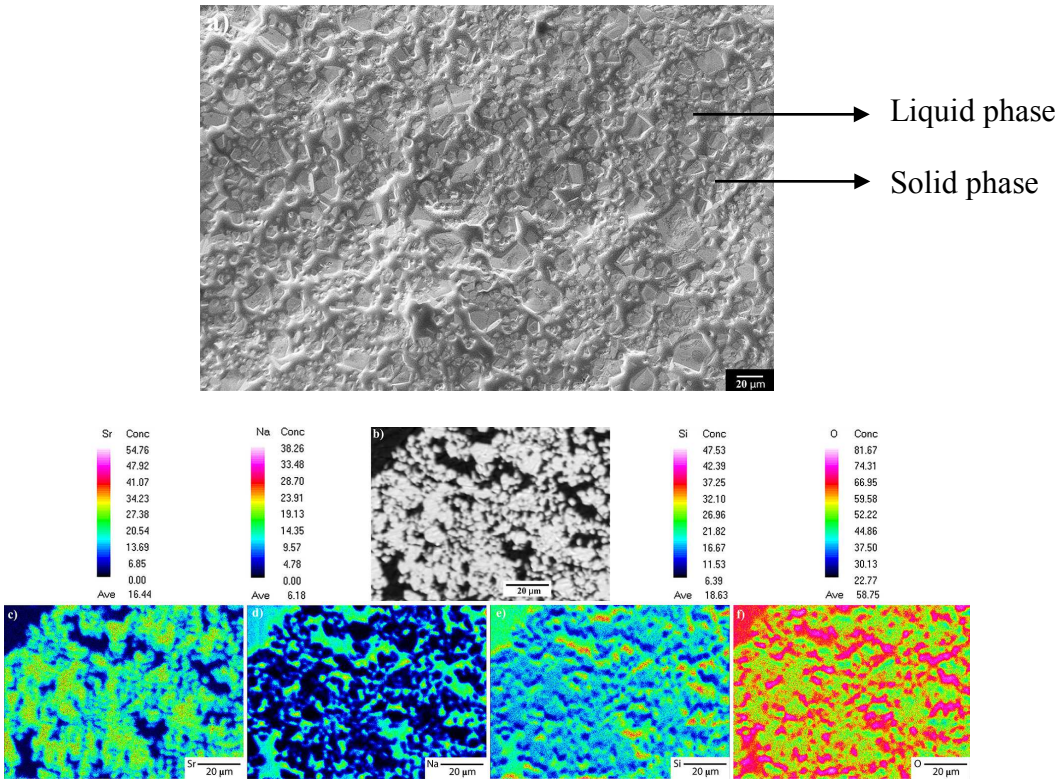

Figure 3. FE-SEM image (a) and WDS mapping of $Sr_{0.55}Na_{0.45}SiO_{3-\delta}$ (b−f).

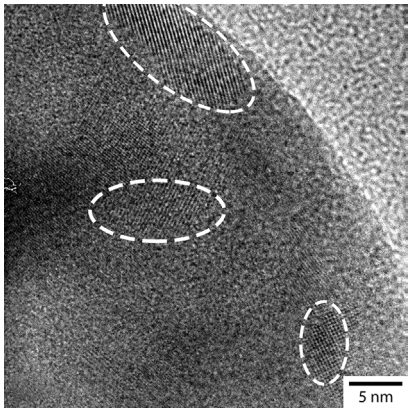

Figure 4. TEM image of $Sr_{0.55}Na_{0.45}SiO_{3-\delta}$.

Impedance Study

Electrochemical impedance spectroscopy (EIS) measures the response of a sample under an alternating current stimulus in which the frequency is varied over a wide range (15). In 1967, Bauerle introduced EIS technique to determine the oxygen ionic conductivity in solid electrolytes (16). Impedance spectra of typical solid oxide fuel cell electrolyte consist of three semicircles. Each semicircle represents a distinct process. The semicircle at high frequency and low frequency represents grain and electrode contribution respectively, while the semicircle at intermediate frequency represents the GB contribution (17). In the absence of clear semicircle at high frequencies as in the present case, the intercept of the linear region of the curve to the real axis is taken to

determine the total conductivity (18). The impedance spectrum is typically represented as negative of imaginary component impedance (-Z″) versus real component of impedance (Z′), which is referred as 'Nyquist plot'. In the measured temperature range (300-700^{0}C), $SrSiO_3$ behaves as an insulator with impedance at different frequencies in the same region. Figure 5 represents the Nyquist plots for $Sr_{0.55}Na_{0.45}SiO_{3-\delta}$ at different temperature. At 300 ^{0}C, $Sr_{0.45}Na_{0.55}SiO_{3-\delta}$ shows both grain and GB contribution (fitted by using (R_1)-(R_2CPE_2) equivalent circuit) and a spike for electrode contribution. As the temperature increases both grain and GB arcs disappears, which may be due to time constant associated with grain and GBs are much smaller when compare to electrode process (17). The conductivity for $Sr_{0.55}Na_{0.45}SiO_{3-\delta}$ at low temperature is due to both grain and GB, while as the temperature increases, the conductivity is mainly due to GB contribution, not due to intra-grain region. Amorphous $Na_2Si_2O_5$ segregates along the GBs as temperature increases, with slightly doped Na-$SrSiO_3$ in the grain region. This observation is further supported by FE-SEM and WDS, which confirms that GBs are Na-rich and grains are Na deficient insulating $SrSiO_3$ phase. Figure 6 shows the variation of conductivity with temperature, which indicates that the conductivity strongly depends on temperature. As the temperature increases the conductivity also increase, which illustrate the acceleration of migration of oxygen ion vacancy. Conductivity (σ) was calculated using the following equation:

$$\sigma = t/RA \quad [1]$$

where, t = thickness**,** A = area and R = resistance of the pellet. The Arrhenius plot for $Sr_{0.55}Na_{0.45}SiO_{3-\delta}$ is shown in Figure 7. From the figure, it can be clearly seen that the experimental data is well fitted with straight line throughout the measured temperature. It also indicates that the conductivity can be expressed in the form of Arrhenius equation

$$\sigma = (\sigma_0/T)\exp(-Ea/k_BT) \quad [2]$$

Where E_a = activation energy, k = Boltzmann constant, σ_0 = pre-exponential factor. The observed conductivity here is lower when compare to Singh et al. (19), the same discrepancy was observed by Bayliss et al. (10) and Evans et al. (20). The activation energy for $Sr_{0.55}Na_{0.45}SiO_{3-\delta}$ is 0.39 eV. The conductivity of $Sr_{0.55}Na_{0.45}SiO_3$ (1.12×10^{-2} S cm^{-1}) at 700 ^{0}C which is higher when compare to other solid electrolytes $La_{0.9}Sr_{0.1}In_{0.8}Mg_{0.2}O_{3-\delta}$ (2.48×10^{-3} S cm^{-1}), $La_{0.9}K_{0.1}Ga_{0.9}Mg_{0.1}O_{3-\delta}$ (8.56×10^{-3} S cm^{-1}) (21) and $La_{0.9}Ca_{0.1}InO_{3-\delta}$ (1.6×10^{-3}S cm^{-1}) (22). Finally, we can conclude that $Sr_{0.55}Na_{0.45}SiO_{3-\delta}$ is rare earth free and inexpensive composite system, with amorphous Na-rich phase ($Na_2Si_2O_5$) along the GBs and Na-$SrSiO_3$ in the grain.

Conclusion

In the present study, $SrSiO_3$ and $Sr_{0.55}Na_{0.45}SiO_{3-\delta}$ were synthesized by solid state reactions. In the measured temperature range, $SrSiO_3$ behaves as insulator, while $Sr_{0.55}Na_{0.45}SiO_{3-\delta}$ shows good ionic conductivity. $Sr_{0.55}Na_{0.45}SiO_{3-\delta}$ contains two phases namely intra-grain $SrSiO_3$ and inter-grain $Na_2Si_2O_5$. The presence of $Na_2Si_2O_5$ is confirmed by NMR, FE-SEM and WDS which is the main reason for the enhanced electrical properties of $Sr_{0.55}Na_{0.45}SiO_{3-\delta}$. Hence, we envisage that $Sr_{0.55}Na_{0.45}SiO_{3-\delta}$ can be used as a potential electrolyte material for IT-SOFCs applications.

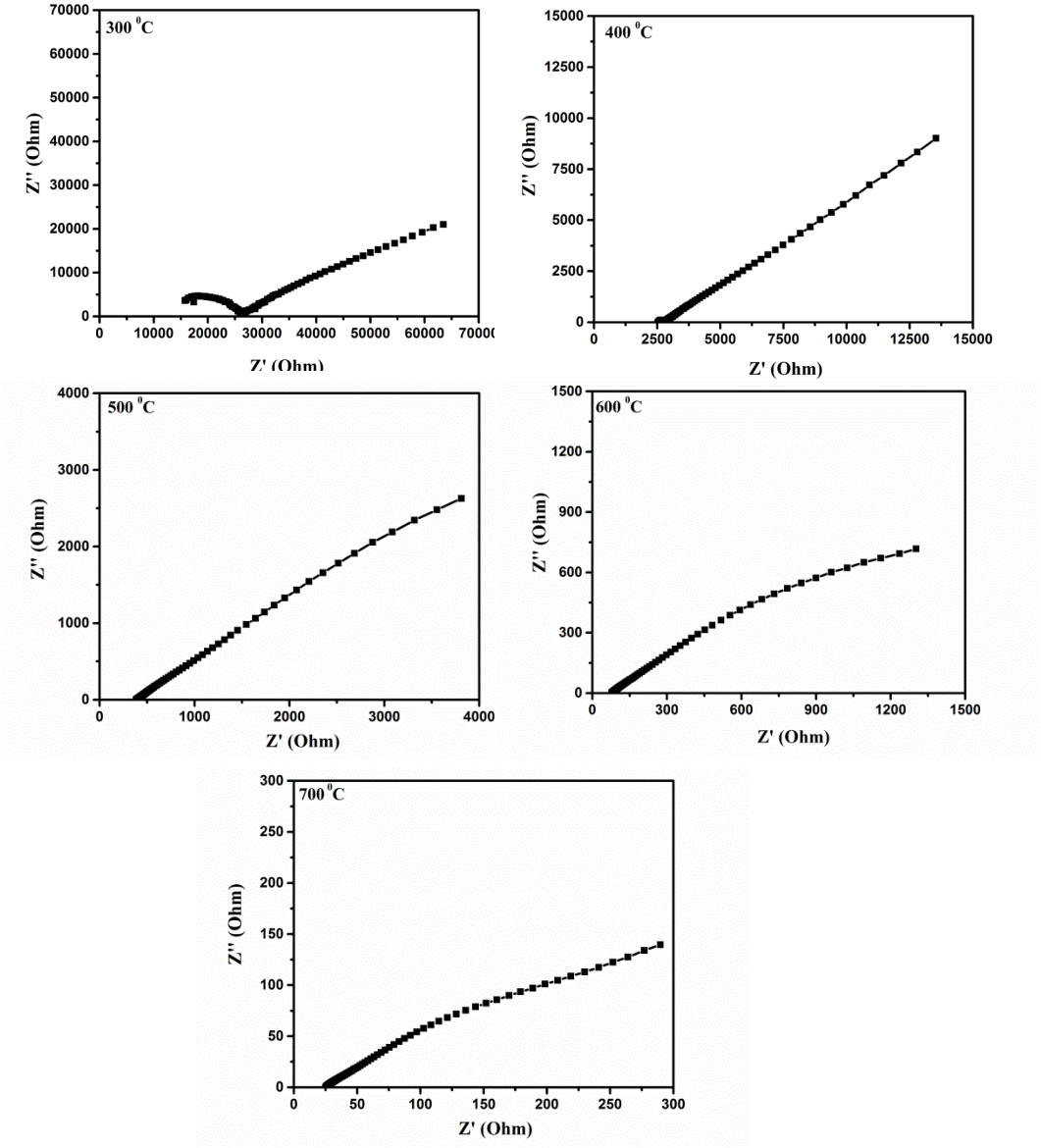

Figure 5. Nyquist plots for $Sr_{0.55}Na_{0.45}SiO_{3-\delta}$ at different temperatures.

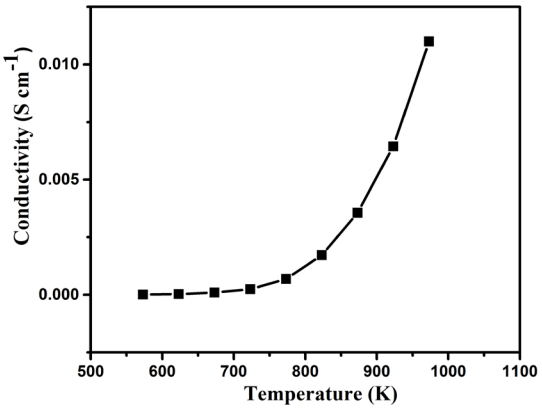

Figure 6. Variation of conductivity of $Sr_{0.55}Na_{0.45}SiO_{3-\delta}$ with temperature.

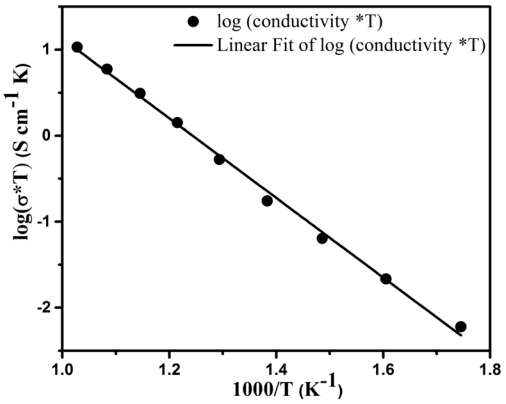

Figure 7. Arrhenius plot for $Sr_{0.55}Na_{0.45}SiO_{3-\delta}$

Acknowledgements

We gratefully acknowledge the financial support from Science and Engineering Research Board (Grant No.: SERB/PDF/2015/1028, Department of Science and Technology, Government of India.

References

1. J. Hou, L. Bi, J. Qian, Z. Gong, Z. Zhu and W. Liu, *J. Power Sources*, **301**, 306 (2016).
2. H. Sun, Y. Chen, F. Chen, Y. Zhang and M. Liu, *J. Power Sources*, **301**, 199 (2016).
3. M. Kahlaoui, A. Inoubli, S. Chefi, A. Mezni, A. Kouki, A. Madaniand C. Chefi, *Int. J. Hydrogen Energy,* **41**, 4751 (2016).
4. J. Will, A. Mitterdorfer, C. Kleinlogel, D. Perednis and L. J. Gauckler, *Solid State Ionics,* **131**, 79 (2000).
5. C. Zuo, S. Zha, M. Liu, H. Hatano and M. Uchiyama, *Adv. Mater.,* **18**, 3318 (2006).
6. W. Sun, Z. Shi, J. Qian, Z. Wang and W. Liu, *Nano Energy,* **8**, 305 (2014).
7. J. W. Fergus, *J. Power Sources*, **162**, 30 (2006).
8. R. Martinez-Coronado, P. Singh, J. Alonso-Alonso and J. B. Goodenough, *J. Mater. Chem. A,* **2**, 4355 (2014).
9. J. Xu, X. Wang, H. Fu, C. M. Brown, X. Jing, F. Liao, F. Lu, X. Li, X. Kuang and M. Wu, *Inorg. Chem.,* **53**, 6962 (2014).
10. R. D. Bayliss, S. N. Cook, S. Fearn, J. A. Kilner, C. Greaves and S. J. Skinner, *Energy Environ. Sci*., **7**, 2999 (2014).
11. R. D. Bayliss, S. N. Cook, D. O. Scanlon, S. Fearn, J. Cabana, C. Greaves, J. A. Kilner and S. J. Skinner, *J. Mater. Chem. A,* **2**, 17919 (2014).
12. F. Nishi, *Acta Crystallogr.,* **C53**, 534 (1997).
13. P. D. Antonio and J. H. Konnert, *Phys. Rev. Lett.,* **43**, 1161 (1979).
14. P. –H, Chien, Y. Jee, C. Huang, R. Dervisoglu, I. Hung, Z. Gan, K. Huang and Y. –Y. Hu, *Chem. Sci.,***7**, 3667 (2016).

15. L. Zhang, F. Liu, K. Brinkman, K. L. Reifsnider and A. V. Virkar, *J. Power Sources*, **247**, 947 (2014).
16. J. E. Bauerle, *J. Phys. Chem. Solids*, **30**, 2657 (1969).
17. G. B. Balazs and R. S. Glass, *Solid State Ionics,* **76**, 155 (1995).
18. K. Jackowska and A. R. West, *J. Mater. Sci.,* **18**, 2380 (1983).
19. P. Singh and J. B. Goodenough, *J. Am. Chem. Soc.,* **5**, 10149 (2013).
20. I. R. Evans, J. S. O. Evans, H. G. Davies, A. R. Haworth and M. L. Tate, *Chem. Mater*. **26**, 5187 (2014).
21. V. Thangadurai and W. Weppner, *J. Electrochem. Soc.,***148** (12), A1294 (2001).
22. K. Sood, K. Singh, S. Basu and O. P. Pandey, *Ionics,* **21**, 2839 (2015).